



Isvector giant monopole and quadrupole resonances in a Skyrme energy density functional approach with axial symmetry

Kenichi Yoshida ^{*}*Department of Physics, Kyoto University, Kyoto 606-8502, Japan* (Received 2 July 2021; revised 8 September 2021; accepted 30 September 2021; published 8 October 2021)

Background: Giant resonance (GR) is a typical collective mode of vibration. The deformation splitting of the isovector (IV) giant dipole resonance is well established. However, the splitting of GRs with other multipolarities is not well understood.

Purpose: I explore the IV monopole and quadrupole excitations and attempt to obtain the generic features of IV giant resonances in deformed nuclei by investigating the neutral and charge-exchange channels simultaneously.

Method: I employ a nuclear energy-density functional (EDF) method: the Skyrme-Kohn-Sham-Bogoliubov and the quasiparticle random-phase approximation are used to describe the ground state and the transition to excited states.

Results: I find the concentration of the monopole strengths in the energy region of the isobaric analog or Gamow-Teller resonance irrespective of nuclear deformation, and the appearance of a high-energy giant resonance composed of the particle-hole configurations of $2\hbar\omega_0$ excitation. Splitting of the distribution of the strength occurs in the giant monopole and quadrupole resonances due to deformation. The lower K states of quadrupole resonances appear lower in energy and possess the enhanced strengths in the prolate configuration, and vice versa in the oblate configuration, while the energy ordering depending on K is not clear for the $J = 1$ and $J = 2$ spin-quadrupole resonances.

Conclusions: The deformation splitting occurs generally in the giant monopole and quadrupole resonances. The K dependence of the quadrupole transition strengths is largely understood by the anisotropy of density distribution.

DOI: [10.1103/PhysRevC.104.044309](https://doi.org/10.1103/PhysRevC.104.044309)

I. INTRODUCTION

The response of a nucleus to an external field induces various modes of excitation, reflecting many-nucleon correlations and internucleon interactions in the nuclear medium. Since the external fields are classified by quantum numbers, the collective modes of motion are selectively excited [1]; the nuclear response is characterized by the transferred angular momentum ΔL , spin ΔS , isospin ΔT , and particle number ΔN .

The isovector (IV) giant dipole resonance (GDR) represented as $\Delta L = 1$, $\Delta S = 0$, $\Delta T = 1$, $\Delta N = 0$ is one of the well studied collective vibrational modes of excitation among various types of giant resonance (GR) [2]. The GDR is an oscillation of protons against neutrons represented as $\Delta T_z = 0$ and can be seen in a wider perspective when it is considered as a single component $\Delta T_z = 0$ of the isovector (IV) dipole modes [3–6]. The additional components $\Delta T_z = \pm 1$ represent the charge-exchange modes. In addition to the Coulomb potential, with the presence of excess neutrons, i.e., deformation in isospin space, the IV strengths reveal the splitting for $\Delta T_z = 0, \pm 1$ [3]. The charge-exchange excitations have attracted interest not only because they reflect the isospin and

spin-isospin character of a nucleus but because they have a relevance for nuclear β decay, thus connecting strong and weak interactions [7]. However, there has been little study of the giant multipole resonances other than the dipole, isobaric analog (IAR), and Gamow-Teller (GTR) resonances [1].

Extensive theoretical works in Refs. [4–6] opened up an avenue of the study for the IV multipole excitations other than $\Delta L = 1$. Nowadays, not only light-ion but heavy-ion charge-exchange reactions have become an effective probe for investigating the multipole excitations, which, using nucleonic probes, are difficult to study [8]. Recent experimental progress has enabled precise measurements of the electric quadrupole resonance [9] and leads to the understanding of the nuclear symmetry energy [10]. Although the IV GRs provide useful insight into the symmetry energy, the isoscalar (IS) part is in some cases dominant in the inelastic scattering reactions with $\Delta T_z = 0$. Since the IS component is absent in the $\Delta T_z = \pm 1$ channels, a detailed investigation of the charge-exchange GRs would give an additional constraint on the symmetry energy. The anti-analog GDR is an example [11–16]. Furthermore, to investigate the isospin structure of the excitation modes, such as the pygmy dipole resonance, a comparative study in the $\Delta T_z = 0$ and -1 channels has been carried out in Refs. [17,18]. However, most of the theoretical studies have been restricted to spherical nuclei except for some attempts in Refs. [19–25] for the $\Delta T_z = 0$ channel.

^{*}kyoshida@ruby.scphys.kyoto-u.ac.jp

The nuclear shape deformation brings about a characteristic feature in the GRs; peak splitting of the GDR, which is caused by the different frequencies of oscillation along the long and short axes, has been observed in experiments [2]. The splitting of the distribution of the strengths has also been investigated in the IS giant multipole resonances represented as $\Delta T = 0$, which is another branch of the GRs [1]. For the monopole $\Delta L = 0$ resonance, the spitting is due to the coupling to the $\Delta L_z = 0$ component of the quadrupole $\Delta L = 2$ resonance [26], which manifests the breaking of the rotational symmetry in the intrinsic frame.

The present work aims to provide a consistent and systematic description of all three modes $\Delta T_z = 0, \pm 1$ of IV excitations for both electric $\Delta S = 0$ and magnetic $\Delta S = 1$ types in a single framework, and to study the spitting of the distribution of the strengths according to ΔT_z and ΔL_z or ΔJ_z associated with deformation in isospin space and real space. Thus, I consider open-shell nuclei where the nuclear deformation occurs in the ground state after demonstrating that the present framework describes the IV responses in spherical nuclei. I use a nuclear energy-density-functional (EDF) method: a theoretical model being capable of handling nuclides with arbitrary mass numbers [27,28],

This paper is organized in the following way: the theoretical framework for describing the nuclear responses is given in Sec. II and the details of the numerical procedures are also given; Sec. III is devoted to the numerical results and discussion based on the model calculation; non-spin-flip electric-type excitations and spin-flip magnetic-type excitations are discussed in Secs. III A and III B, respectively; then, a summary is given in Sec. IV.

II. THEORETICAL MODEL

A. Kohn-Sham-Bogoliubov and quasiparticle random-phase approximation calculations

Since the details of the formalism can be found in Refs. [21,29–31], here I briefly recapitulate the basic equations relevant to the present study. In the framework of the nuclear EDF method I employ, the ground state of a mother (target) nucleus is described by solving the Kohn-Sham-Bogoliubov (KSB) equation [32]:

$$\sum_{s'} \begin{bmatrix} h_{ss'}^q(\mathbf{r}) - \lambda^q \delta_{ss'} & \tilde{h}_{ss'}^q(\mathbf{r}) \\ \tilde{h}_{ss'}^q(\mathbf{r}) & -h_{ss'}^q(\mathbf{r}) + \lambda^q \delta_{ss'} \end{bmatrix} \begin{bmatrix} \varphi_{1,\alpha}^q(\mathbf{r}s') \\ \varphi_{2,\alpha}^q(\mathbf{r}s') \end{bmatrix} = E_\alpha \begin{bmatrix} \varphi_{1,\alpha}^q(\mathbf{r}s) \\ \varphi_{2,\alpha}^q(\mathbf{r}s) \end{bmatrix}, \quad (1)$$

where the single-particle and pair Hamiltonians, $h_{ss'}^q(\mathbf{r})$ and $\tilde{h}_{ss'}^q(\mathbf{r})$, are given by the functional derivative of the EDF with respect to the particle density and the pair density, respectively. An explicit expression of the Hamiltonians is found in the Appendix of Ref. [33]. The superscript q denotes ν (neutron, $t_z = 1/2$) or π (proton, $t_z = -1/2$). The average particle number is fixed at the desired value by adjusting the chemical potential λ^q . Assuming the system is axially symmetric, the KSB equation (1) is block diagonalized according

to the quantum number Ω , the z component of the angular momentum.

The excited states $|i\rangle$ are described as one-phonon excitations built on the ground state $|0\rangle$ of the mother nucleus as

$$|i\rangle = \hat{\Gamma}_i^\dagger |0\rangle, \quad (2)$$

$$\hat{\Gamma}_i^\dagger = \sum_{\alpha\beta} \{X_{\alpha\beta}^i \hat{a}_\alpha^\dagger \hat{a}_\beta^\dagger - Y_{\alpha\beta}^i \hat{a}_\beta \hat{a}_\alpha\}, \quad (3)$$

where \hat{a}^\dagger and \hat{a} are the quasiparticle (qp) creation and annihilation operators that are defined in terms of the solutions of the KSB equation (1) with the Bogoliubov transformation. The phonon states, the amplitudes X^i, Y^i and the vibrational frequency ω_i , are obtained in the quasiparticle random-phase approximation (QRPA): the linearized time-dependent density-functional theory for superfluid systems [28]. The EDF gives the residual interactions entering into the QRPA equation. For the axially symmetric nuclei, the QRPA equation is block diagonalized according to the quantum number $K = \Omega_\alpha + \Omega_\beta$.

B. Numerical procedures

I solve the KSB equation in the coordinate space using cylindrical coordinates $\mathbf{r} = (\varrho, z, \phi)$. Since I assume further the reflection symmetry, only the region of $z \geq 0$ is considered. I use a two-dimensional lattice mesh with $\varrho_i = (i - 1/2)h$, $z_j = (j - 1)h$ ($i, j = 1, 2, \dots$) with a mesh size of $h = 0.6$ fm and 25 points for each direction. The qp states are truncated according to the qp energy cutoff at 60 MeV, and the qp states up to the magnetic quantum number $\Omega = 23/2$ with positive and negative parities are included. I introduce the truncation for the two-quasiparticle (2qp) configurations in the QRPA calculations, in terms of the 2qp energy as 70 MeV. The calculated energy and transition strength of the low-lying and giant resonance states are almost converged with respect to the mesh size, the box size, and the energy cutoff [29], and are compatible with the results obtained in different methodology [22,34].

For the normal (particle-hole) part of the EDF, I employ the SkM* functional [35]. For the pairing energy, I adopt the so-called mixed-type interaction:

$$V_{\text{pair}}^q(\mathbf{r}, \mathbf{r}') = V_0 \left[1 - \frac{\rho(\mathbf{r})}{2\rho_0} \right] \delta(\mathbf{r} - \mathbf{r}') \quad (4)$$

with $\rho_0 = 0.16$ fm $^{-3}$, and $\rho(\mathbf{r})$ being the isoscalar (matter) particle density. I use the parameter V_0 as fixed in the previous studies: $V_0 = -275$ MeV fm 3 for the Mg and Si isotopes [36], $V_0 = -240$ MeV fm 3 for the Ni, Zr, and Pb isotopes [20]. For the pairing energy of the Sm isotopes, I adopt the one in Ref. [37] that depends on both the IS and IV densities, in addition to the pair density, with the parameters given in Table III of Ref. [37]. The same pair interaction is employed for the dynamical pairing in the QRPA calculation and for the $S = 0$ and $S = 1$ proton-neutron pairing in the pnQRPA calculation, while the linear term in the IV density is dropped. Note that the pnQRPA calculations including the dynamic spin-triplet pairing with more or less the same strength as the spin-singlet pairing describe well the characteristic low-lying Gamow-

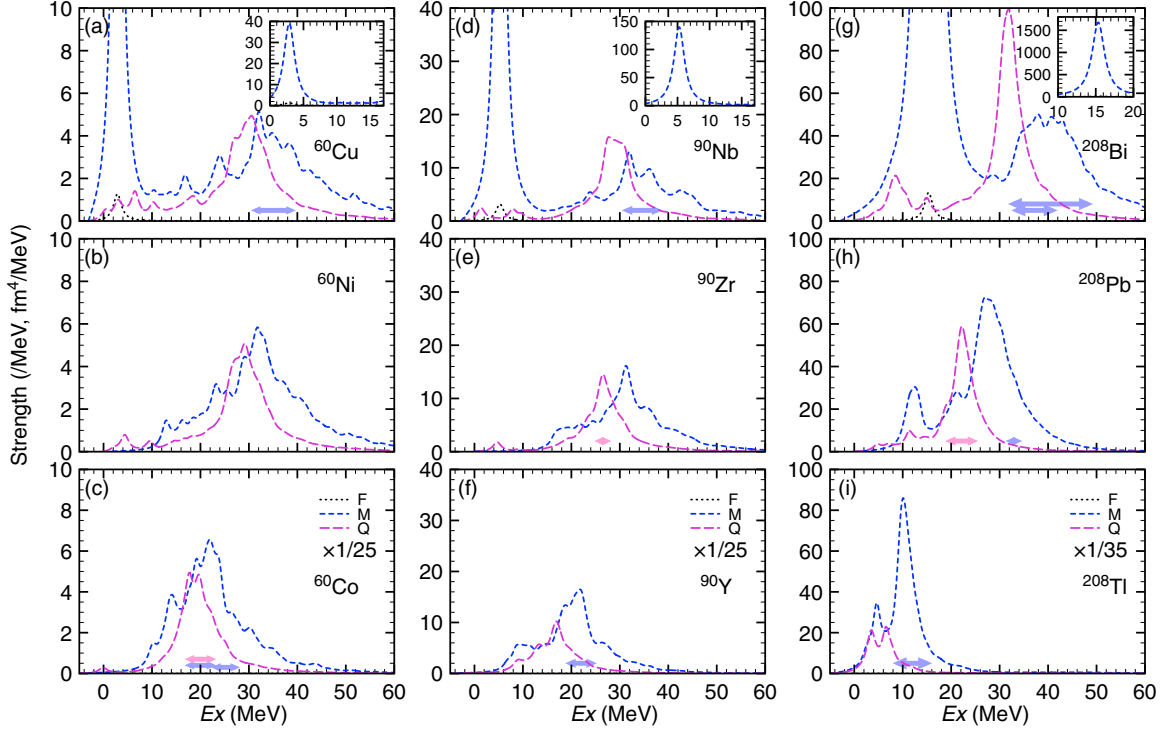


FIG. 1. Transition strengths of the non-spin-flip excitations in the $\mu = -1$ [(a), (d), (g)], $\mu = 0$ [(b), (e), (h)], and $\mu = +1$ channels [(c), (f), (i)]. The Fermi (F), monopole (M), and quadrupole (Q) strengths are shown by the dotted, dashed, and long-dashed lines, respectively. The quadrupole strengths are multiplied by $1/25$ ($1/35$ for ^{208}Bi , Pb , Tl). The excitation energies E_x are with respect to the ground state of the daughter nucleus. Arrows indicate the experimental data for the excitation energy.

Teller strength distributions in the light $N \simeq Z$ nuclei [38–40], and the β -decay half-lives of neutron-rich Ni isotopes [41]. Furthermore, the present theoretical framework describes well the measured giant resonances in light, medium-heavy, and heavy nuclei [21,36,42–48], and low-lying collective modes of vibration [21,49–53].

C. Strength distribution

I investigate the nuclear responses by looking at the transition-strength distribution:

$$S_L^\mu(E) = \sum_K \frac{dB(E, F_{LK\mu})}{dE}, \quad (5)$$

$$\frac{dB(E, F_{LK\mu})}{dE} = \frac{2E\gamma}{\pi} \sum_i \frac{\tilde{E}_i |\langle i | \hat{F}_{LK\mu}^{(e,m)} | 0 \rangle|^2}{(E^2 - \tilde{E}_i^2)^2 + E^2\gamma^2}, \quad (6)$$

where $\tilde{E}_i^2 = (\hbar\omega_i)^2 + \gamma^2/4$ [3]. The operators $\hat{F}^{(e,m)}$ are defined below. The smearing width γ is set to 2 MeV, which is supposed to simulate the spreading effect, Γ^\downarrow , missing in the QRPA. The escaping effect, Γ^\uparrow , is approximately taken into account using the discretized continuum states in a box. Then, the sum of strengths is defined as

$$m_L^\mu = \int dE S_L^\mu(E). \quad (7)$$

III. RESULTS AND DISCUSSION

A. Electric modes: Non-spin-flip excitations

I consider the response to the IV operators defined by

$$\hat{F}_{LK\mu}^{(e)} = \frac{1}{\sqrt{2}} \sum_{ss'} \sum_{tt'} \int dr f(r) Y_{LK}(\hat{r}) \delta_{ss'} \langle t' | \tau_\mu | t \rangle \times \hat{\psi}^\dagger(\mathbf{r}s't') \hat{\psi}(\mathbf{r}st), \quad (8)$$

where $\hat{\psi}^\dagger(\mathbf{r}st)$, $\hat{\psi}(\mathbf{r}st)$ represent the nucleon field operators, and $\vec{\tau} = (\tau_{+1}, \tau_0, \tau_{-1})$ denotes the spherical components of the Pauli matrix of isospin. I take $f(r) = \sqrt{4\pi}$ for the Fermi (F, $L = 0$) transition, while r^2 for the monopole (M, $L = 0$) and quadrupole (Q, $L = 2$) transitions.

1. Spherical nuclei

Before investigating deformed nuclei, I study the IV giant resonances in some spherical nuclei, where the experimental data are available. Figure 1 shows the transition-strength distributions in ^{60}Ni , ^{90}Zr , and ^{208}Pb as an example of spherical nuclei. For the charge-exchange modes of excitation, the excitation energy with respect to the ground state of the mother nucleus is evaluated by replacing E by $E \pm (\lambda^\nu - \lambda^\pi)$ for the $\mu = \pm 1$ channel [54]. Furthermore, in plotting the strength distributions with respect to the ground state of the daughter nucleus, the mass difference between the mother and daughter is considered by using AME2020 [55,56]: the ground-state Q value is -6.1 and -2.8 MeV in ^{60}Cu and ^{60}Co with respect

TABLE I. Summed monopole and quadrupole strengths, and comparison with the non-energy-weighted sum rule (NEWSR) values, given in units of fm^4 . $\langle r^4 \rangle$ for neutrons (protons) is 276 (257) fm^4 , 444 (421) fm^4 , and 1284 (1114) fm^4 in ^{60}Ni , ^{90}Zr , and ^{208}Pb , respectively. The summed monopole strengths excluding the strength of the IAR are given in the parentheses.

	m_L^{-1}	m_L^{+1}	m_L^0	$m_L^{-1} - m_L^{+1}$	NEWSR
^{60}Ni					
$L = 0$	228.3 (107.1)	97.00	107.3	131.3	131.1
$L = 2$	1901	1242	1546	658.6	655.4
^{90}Zr					
$L = 0$	639.2 (202.2)	212.2	217.8	427.0	425.8
$L = 2$	4427	2289	3259	2138	2129
^{208}Pb					
$L = 0$	6210 (952.3)	599.6	1044	5610	5607
$L = 2$	33734	5681	16063	28053	28036

to ^{60}Ni , -6.1 and -2.2 MeV in ^{90}Nb and ^{90}Y with respect to ^{90}Zr , and -2.9 and -5.0 MeV in ^{208}Bi and ^{208}Tl with respect to ^{208}Pb .

A striking feature one sees in the $\mu = -1$ channel is the concentration of the monopole strength in the isobaric analog resonance (IAR). I find 53%, 68%, and 85% of the total strength in the IAR in ^{60}Cu , ^{90}Nb , and ^{208}Bi , respectively, as summarized in Table I. It is noted that the summed strengths excluding the IAR are given in parentheses in Table I. A similar trait was also found in the early investigation [4]. In the high-frequency region, the peak energy of the monopole resonance is higher than the quadrupole resonance. This is also the case in the $\mu = 0$ and $\mu = +1$ channels. Furthermore, the strengths are spread out over a wider energy region for the monopole resonance; the width of the isovector giant monopole resonance (IVGMR) is larger than that of the isovector giant quadrupole resonance (IVGQR).

Table I lists the summed strengths for the monopole and quadrupole excitations. One can see that the present calculation satisfies the model-independent non-energy-weighted sum rule for the charge-exchange modes [3]:

$$m_L^{-1} - m_L^{+1} = \begin{cases} N - Z, & \text{F,} \\ \frac{2L+1}{4\pi} (N\langle r^4 \rangle_\nu - Z\langle r^4 \rangle_\pi), & \text{M, Q,} \end{cases} \quad (9)$$

where $\langle r^4 \rangle_{\nu(\pi)}$ stands for the expectation value evaluated for neutrons (protons) in the ground state of the mother nucleus. In these nuclei, m^{-1} is always larger than m^{+1} because $\langle r^4 \rangle$ for neutrons is slightly larger than that for protons. The monopole and quadrupole excitations are primarily built of a coherent particle-hole configurations of $2\hbar\omega_0$ excitation, and the high-frequency resonance is such a mode of excitation. However, the $0\hbar\omega_0$ excitation can also be involved.

For the monopole excitations, the $\nu 2p_{3/2} \rightarrow \pi 2p_{3/2}$ and $\nu 1g_{9/2} \rightarrow \pi 1g_{9/2}$ excitation generates the IAR of ^{60}Ni and ^{90}Zr , while the $0\hbar\omega_0$ excitation is strongly suppressed in the $\mu = +1$ channel due to the Pauli blocking. The summed strength m^{-1} excluding the IAR has a value similar to m^0 and

m^{+1} . This indicates that the higher-energy monopole strengths in the $\mu = -1$ channel represent the $2\hbar\omega_0$ excitation. In ^{208}Pb , the summed strength m^{-1} excluding the IAR has a value similar to m^0 . This again indicates that the higher-energy monopole strengths in the $\mu = -1$ channel correspond to the $2\hbar\omega_0$ excitation. As mentioned above, the spreading effect is not included in the present framework. In Ref. [57], the IV monopole resonance in ^{208}Tl was investigated, taking the coupling to the two-particle–two-hole configurations into consideration. The distribution is composed of basically two peaks, with the higher-energy resonance having a broad width. The present calculation produces the excitation energy with a qualitative agreement with the results of Ref. [57].

The quadrupole excitation is very complicated. In ^{60}Ni , the $1f_{7/2} \rightarrow 1f_{5/2}$ excitation is available in all the channels. The $\nu 1p_{3/2} \rightarrow \pi 1p_{3/2}$ excitation participates in the low-lying 2^+ excitation in the $\mu = -1$ channel, and the $1p_{3/2} \rightarrow 1p_{1/2}$ excitation further contributes to generate the 2^+ excitation in the $\mu = -1$ and $\mu = 0$ channels. Thus, the 2^+ states appear at low energy with the transition strengths dependent on μ . In ^{90}Zr , the $1g_{9/2} \rightarrow 1g_{7/2}$ excitation generates the low-lying 2^+ excitation in the $\mu = 0$ and $\mu = -1$ channel. Furthermore, the $\nu 1g_{9/2} \rightarrow \pi 1g_{9/2}$ excitation participates in the low-lying 2^+ excitation in the $\mu = -1$ channel. Therefore, one sees the strengths at low energy, while there are no strengths in the $\mu = +1$ channel since the $0\hbar\omega_0$ excitation is not available. In ^{208}Pb , both $0\hbar\omega_0$ and $2\hbar\omega_0$ excitations generate the 2^+ excitation in the $\mu = -1$ channel, acquiring a large strength. In the $\mu = 0$ channel, the $\pi 1h_{11/2} \rightarrow \pi 1h_{9/2}$ and $\nu 1i_{13/2} \rightarrow \nu 1i_{11/2}$ excitations as well as the $2\hbar\omega_0$ excitation generate the 2^+ excitation. However, the $0\hbar\omega_0$ excitation is unavailable in the $\mu = +1$ channel. Therefore, the transition strengths in the $\mu = +1$ channel are smaller than in the other channels as in the monopole case.

Here, I compare the calculated strength distributions with the available experimental data. A systematic study of the charge-exchange (π^\pm, π^0) reaction reveals the IVGMR in medium-mass and heavy nuclei [58]: the excitation energy of the IVGMR measured using the $^{208}\text{Pb}(\pi^+, \pi^0)^{208}\text{Bi}$ reaction is 37.2 ± 3.5 MeV, while $E_x = 12.0 \pm 2.8$ MeV in $^{208}\text{Pb}(\pi^-, \pi^0)^{208}\text{Tl}$. The excitation energies in lighter nuclei are $E_x = 35.6 \pm 2.8$ and 25.2 ± 1.7 MeV for ^{60}Cu and ^{60}Co and $E_x = 34.6 \pm 2.9$ and 22.0 ± 2.0 MeV for ^{90}Nb and ^{90}Y . The inelastic electron scattering experiment suggests the resonance around 33 MeV in ^{208}Pb as the IVGMR [59], though this is ≈ 5 MeV higher than the average of E_{T-1} and E_{T+1} obtained using the charge-exchange reaction. The nuclear reactions have also been employed to measure the IVGMR. The $\text{Pb}(^3\text{He}, t\text{p})\text{Bi}$ reaction indicates the location of the IVGMR or spin monopole resonance at 30–45 MeV with respect to the ground state of Pb [60]. The IVGMR measured using the ($^7\text{Li}, ^7\text{Be}$) reaction is found at 20 ± 2 MeV in ^{60}Co [61]. In most cases, the present calculation describes well the location of the IVGMR.

The IVGQR has been found around $130 \times A^{-1/3}$ MeV in the $\mu = 0$ channel [1]. In ^{208}Pb , the excitation energy is 20–23 MeV [9,62–64]. The IVGQR in ^{90}Zr is located around 26–27 MeV [65,66]. The present calculation employing the SkM* functional reproduces well these experimental data.

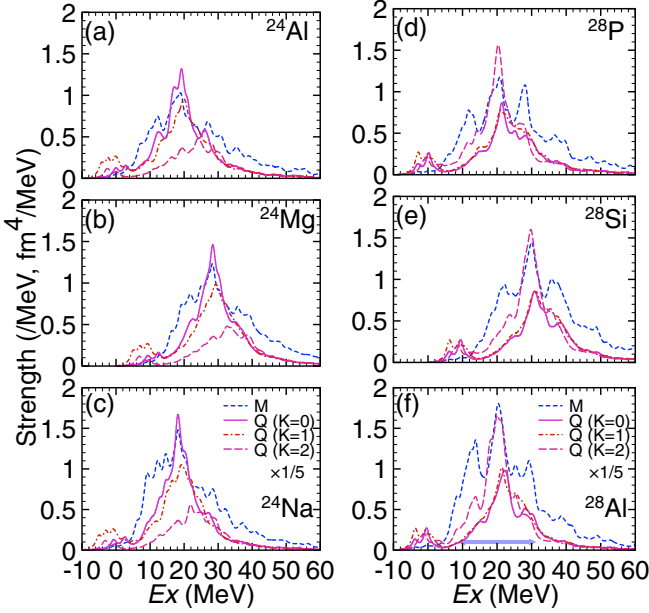


FIG. 2. As in Fig. 1 but for the deformed ^{24}Mg and ^{28}Si nuclei. Instead of showing the total strengths, those for each K component are shown for the quadrupole excitations. The quadrupole strengths are multiplied by $1/5$.

The (^{13}C , ^{13}N) reaction has been employed to locate the IVGQR in ^{60}Co , and it is found at $E_x = 20 \pm 2$ MeV [67]. The calculation is in remarkable agreement with the experiment, as shown in Fig. 1(c)

2. Deformation effects

I am going to investigate the deformation effects. Figure 2 shows the transition-strength distributions in ^{24}Mg and ^{28}Si as an example of light deformed nuclei. As discussed in Refs. [36,45–47], the ground state is prolately deformed and oblately deformed with the deformation parameter $\beta_2 = 0.39$ and -0.22 in ^{24}Mg and ^{28}Si , respectively. Since these nuclei have the same number of protons and neutrons, the Fermi transition strength is weak. A characteristic feature of these $N = Z$ nuclei is that the transition strength distributions in the three channels are similar to each other. For the dipole case, this characteristic trait has been discussed in Ref. [18]. Without the Coulomb potential, one cannot distinguish the motion of protons and neutrons in $N = Z$ nuclei, and the isotriplet states degenerate. However, the Coulomb potential slightly expands the proton distribution, which leads to the asymmetry, as expected by the sum rule (9). A simple RPA analysis for a single normal mode employing the separable interaction gives the relation for the summed transition strengths as [3]

$$\frac{1}{2}(m^{-1} + m^{+1}) = \left[1 + O\left(\frac{N-Z}{A}\right)\right]m^0. \quad (10)$$

In deformed nuclei, the K splitting occurs for the multipole modes of excitation, and thus the sum rule (9) for the

TABLE II. As in Table I but for ^{24}Mg and ^{28}Si .

	m_L^{-1}	m_L^{+1}	m_L^0	$m_L^{-1} - m_L^{+1}$	NEWSR
^{24}Mg					
$L = 0$	23.27	29.25	26.20	-5.98	-6.01
$L = 2, K = 0$	86.94	95.77	91.40	-8.83	-8.93
$L = 2, K = 1$	80.47	87.56	84.32	-7.09	-7.18
$L = 2, K = 2$	45.32	48.68	47.04	-3.36	-3.39
^{28}Si					
$L = 0$	26.82	34.67	30.66	-7.84	-7.87
$L = 2, K = 0$	65.43	71.66	68.64	-6.23	-6.29
$L = 2, K = 1$	73.32	79.62	76.54	-6.30	-6.35
$L = 2, K = 2$	93.86	104.0	99.02	-10.12	-10.18

quadrupole excitation is generalized by replacing $\langle r^4 \rangle$ with

$$\begin{aligned} & \frac{5}{4} \langle 4z^4 + \rho^4 - 4\rho^2 z^2 \rangle, Q(K=0), \\ & \frac{15}{2} \langle \rho^2 z^2 \rangle, Q(K=\pm 1), \\ & \frac{15}{8} \langle \rho^4 \rangle, Q(K=\pm 2), \end{aligned} \quad (11)$$

depending on the K quantum number. Table II summarizes the summed strengths in ^{24}Mg and ^{28}Si , and the NEWSR values taking the nuclear deformation into account (11). One finds that in both nuclei the relation (10) holds accurately. It should be noted that the relation (10) is model dependent. However, the present self-consistent model satisfies the simple relation, suggesting that the relation (10) is a rather general rule for the IV excitations.

As mentioned above, the ^{24}Mg and ^{28}Si nuclei have different shapes in the ground states: prolate deformation in ^{24}Mg and oblate deformation in ^{28}Si . As a consequence of the prolate (oblate) deformation, distinctive features show up in the quadrupole strength distributions at high energy. The $K = 0$ ($K = 2$) states move toward low energy and acquire more considerable strengths in the prolately (oblately) deformed configuration. Furthermore, the coupling to the $K = 0$ component of the IVGQR brings about the resonance peak in the IVGMR. These features are common to the IS excitation. The enhancement of the $K = 0$ ($K = 2$) strengths in the prolate (oblate) configuration, which is also seen in Table II, may be understood by looking at the summed strengths (11): a balance of the terms in Eq. (11) determines the relative strengths. In a prolately (oblately) deformed state, $\langle z^4 \rangle$ increases (decreases), while $\langle \rho^4 \rangle$ decreases (increases), though the evaluation of $\langle \rho^2 z^2 \rangle$ requires a detail of the density distribution.

In Ref. [68], the $^{28}\text{Si}(^{10}\text{Be}, ^{10}\text{B}^*)$ reaction has been employed to identify the IVGMR in a deformed nucleus. The differential cross section displays a broad peak ranging from 10 to 30 MeV in ^{28}Al . The present calculation reasonably explains the measurement. However, it is not easy to find unique features due to deformation as the strength distribution is spread over a wide energy range.

The coupling between the GMR and the $K = 0$ component of the GQR becomes strong in a strongly deformed nucleus,

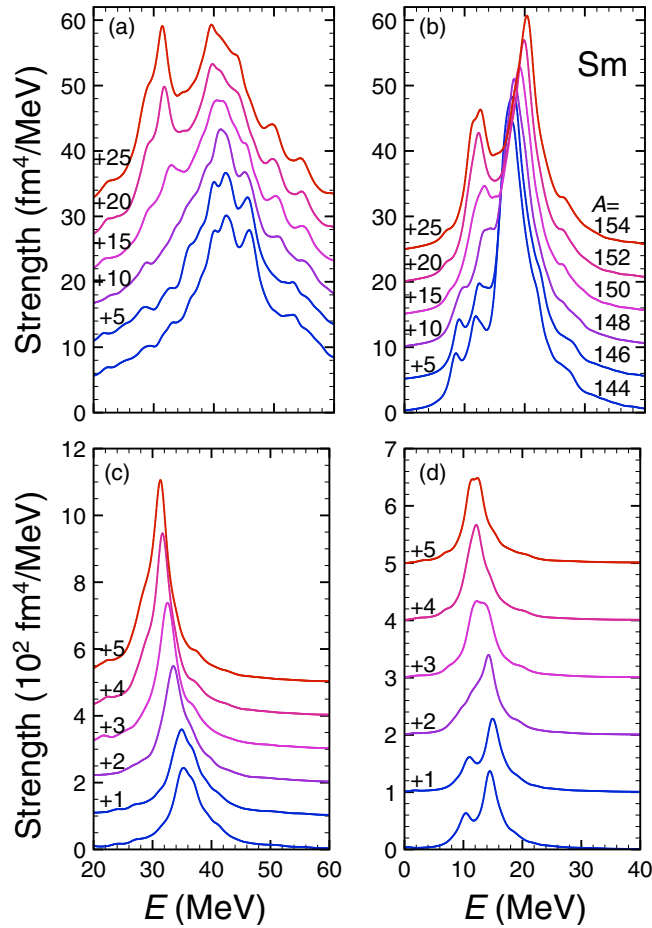


FIG. 3. Monopole strengths in the (a) $\mu = -1$ channel and (b) $\mu = +1$ channel of the Sm isotopes (shifted), and the $K = 0$ component of quadrupole strength distributions in the (c) $\mu = -1$ channel and (d) $\mu = +1$ channel (shifted). The excitation energies are with respect to the ground state of the target nuclei.

which has been investigated for the ISGMR in detail from light to medium-heavy nuclei [26]. The deformation effect on the coupling has also been investigated theoretically for the IVGMR [20,21]: in the $\mu = 0$ channel, the IVGMR shows up at about 30 MeV and the IVGQR around 25 MeV in the Nd and Sm isotopes; see Figs. 6(b) and 6(d) of Ref. [21]. In ^{154}Sm , which is strongly deformed, a resonance peak appears around 20 MeV and one finds clearly the splitting of the monopole strengths [21]. Because the study in Ref. [21] is restricted to the $\mu = 0$ channel, I investigate the deformation effect on the coupling in the $\mu = \pm 1$ channels and to see if the coupling between the GMR and the $K = 0$ component of the GQR is a general feature emerging in deformed nuclei.

Figures 3(a) and 3(b) show the monopole strength distributions in the $\mu = -1$ and $\mu = +1$ channels of the Sm isotopes. Here, the excitation energies are with respect to the ground state of the targets: the Sm isotopes. The IARs are excluded in plotting the strength distribution for the monopole strengths in the $\mu = -1$ channel, because most of the strengths are found in the IAR. One sees that a lower-energy resonance shows up around 30 MeV in $^{150,152,154}\text{Sm}$, while there appears

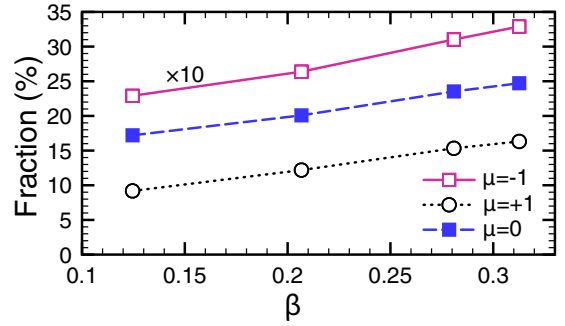


FIG. 4. Fraction of the monopole strengths found in the peak energy region of the $K = 0$ component of the quadrupole strength distribution as a function of the quadrupole deformation parameter in the deformed Sm isotopes with $N = 86-92$.

a resonance around 40–50 MeV in all the isotopes, which is considered as a primal IVGMR. The SkM* functional produces the onset of quadrupole deformation in between $N = 84$ and 86, and the deformation gradually develops with an increase in the neutron number [43]. A similar feature can be seen in the $\mu = +1$ channel: one sees a resonance around 20–25 MeV in all the Sm isotopes, and a prominent peak appears in $^{152,154}\text{Sm}$ at low energy $\approx 10-15$ MeV. The $K = 0$ component of the IVGQR in these isotopes has a peak around 10–15 MeV, as shown in Fig. 3(d), where the lower-energy resonance of the monopole strengths shows up.

The coupling is not only seen in the peak energy but in the transition strengths. Figure 4 shows the fraction of the monopole strengths found in the energy range $[E_{K=0} - 2 \text{ MeV}, E_{K=0} + 2 \text{ MeV}]$, with $E_{K=0}$ being the peak energy of the $K = 0$ component of the quadrupole strength distribution. The $K = 0$ component of the quadrupole strengths is shown in Figs. 3(c) and 3(d). Since most of the monopole strengths are concentrated in the IAR, a factor of 10 is multiplied in plotting the fraction of the $\mu = -1$ channel. The stronger the ground-state deformation, the more enhanced the transition strengths in the lower energy region. Thus, one finds that the monopole resonance at low energy is strongly coupled with the $K = 0$ component of the IVGQR in the well-deformed isotopes.

The coupling is governed by the shell effect and/or the residual interaction. To investigate their roles, I show in Fig. 5 the distributions of the monopole and the $K = 0$ component of the quadrupole strengths in ^{154}Sm . Here, the unperturbed strengths are shown together with those obtained using the QRPA. As already seen above, the lower-energy peak of the monopole strength distribution appears at the peak energy of the $K = 0$ component of the quadrupole strength distribution in all the channels. One can see that the deformation-induced coupling occurs at the mean-field level as a static effect. In the $\mu = -1$ channel, a two-humped structure appears in the monopole strengths; the lower peak is located at the peak energy of the $K = 0$ quadrupole strength distribution. Similarly, the appearance of a small peak structure at low energy ≈ 9 MeV in the monopole strength distribution coincides with the peak of the $K = 0$ quadrupole strength distribution in the $\mu = +1$ channel. In the $\mu = 0$ channel, we have unperturbed

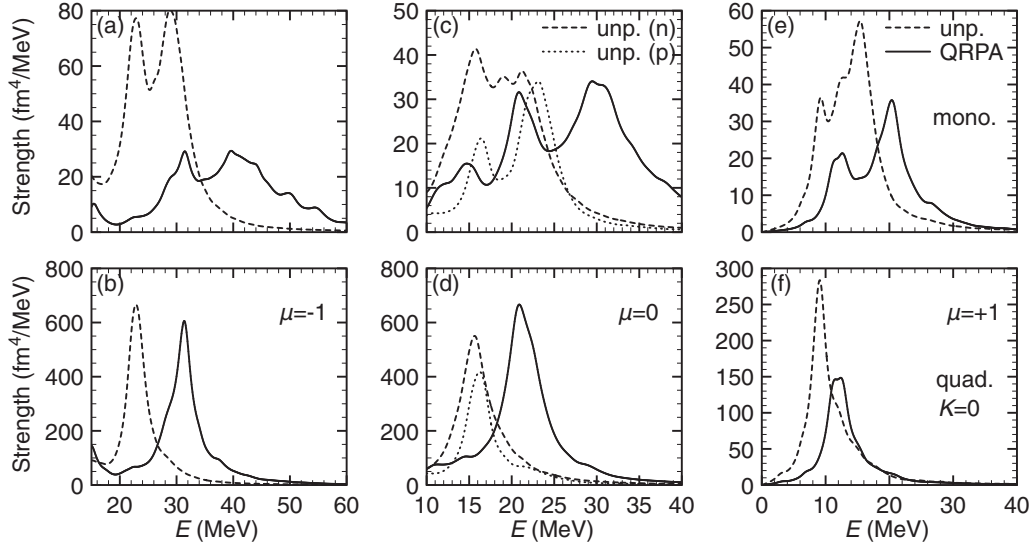


FIG. 5. Distributions of the monopole (upper) and the $K = 0$ component of the quadrupole (lower) strengths in the $\mu = -1$ (a),(b), $\mu = 0$ (c),(d), and $\mu = +1$ (e), (f) channels in ^{154}Sm . The unperturbed strengths are also shown.

strengths of neutrons and protons. The $K = 0$ quadrupole strength distribution has a peak around 15 MeV both for neutrons and protons, with the peak of protons appearing slightly higher in energy than that of neutrons. Accordingly, one sees a lower-energy peak in the monopole strength distribution of neutrons and protons. The monopole and the $K = 0$ quadrupole peaks coincide in energy due to the static deformation effect, where the total angular momentum J is not a good quantum number but K is. The coexistence persists after the residual interaction is applied, and appears as the coupling between the monopole and the $K = 0$ component of the quadrupole resonances. An additional reason for the appearance of the lower-energy peak in the monopole strength distribution is that the $K = 0$ quadrupole strength distribution has a clear peak structure. If the $K = 0$ quadrupole strength distribution were broadened, the lower-energy peak of the monopole strength distribution could be washed out. This brings about the difference between the electric and magnetic monopole modes, as discussed below.

B. Magnetic modes: Spin-flip excitations

Here, I consider the response to the IV operators defined by

$$\hat{F}_{JK\mu}^{(m)} = \frac{1}{\sqrt{2}} \sum_{ss'} \sum_{tt'} \int dr f(r) [Y_L \otimes \vec{\sigma}]_K^j (t' | \tau_\mu | t) \times \hat{\psi}^\dagger(rs't') \hat{\psi}(rst), \quad (12)$$

where $[Y_L \otimes \vec{\sigma}]_K^j = \sum_{vv'} \langle L v 1 v' | JK \rangle Y_{Lv}(\hat{r}) \langle s' | \sigma_{v'} | s \rangle$ with the spherical components of the Pauli spin matrix $\vec{\sigma} = (\sigma_{+1}, \sigma_0, \sigma_{-1})$. I take $f(r) = \sqrt{4\pi}$ for the GT ($L = 0$) transition, while r^2 for the monopole ($L = 0$) and quadrupole ($L = 2$) transitions as in the electric cases. The $J = 3$ spin-quadrupole (SQ) excitation in the $\mu = 0$ channel corresponds to the spin- $M3$ excitation apart from a factor. However, in the present model, the quenching of the transition strength of

the magnetic (spin-flip) modes cannot be described because the tensor force and the meson-exchange currents are not considered.

Early extensive works on the spin monopole (SM) responses in Refs. [6,69] employing Skyrme EDFs revealed that the coupling between the GT and SM states is strong and the excitation energy of the SM resonance (SMR) decreases as the neutron excess in the $\mu = +1$ channel. I investigate these features in deformed nuclei. Before that, I study the SQ excitations in some spherical nuclei.

1. Spin quadrupole excitations in spherical nuclei

Figure 6 shows the transition-strength distributions in ^{90}Zr and ^{208}Pb as an example of spherical nuclei. As in the electric

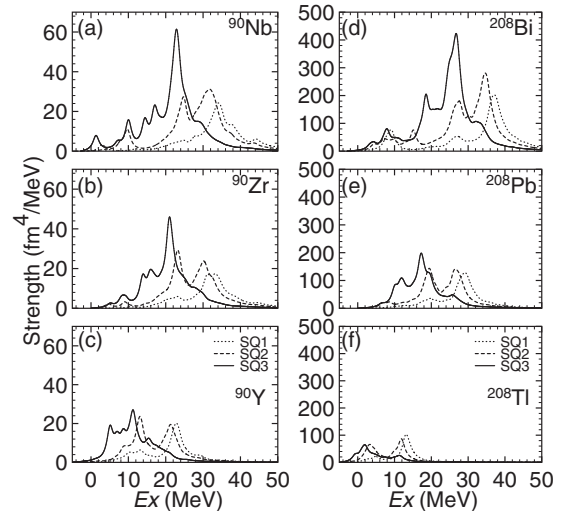


FIG. 6. As in Fig. 1 but for the spin quadrupole (SQ) strengths. The $J = 1, 2,$ and 3 states are depicted by the dotted, dashed, and solid lines, respectively.

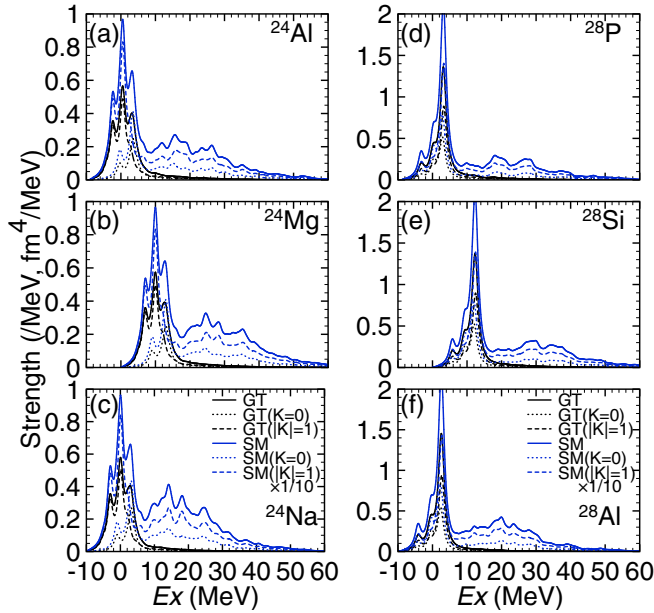


FIG. 7. As in Fig. 2 but for the Gamow-Teller and spin-monopole (SM) excitations. The strengths of $K = \pm 1$ are summed for $|K| = 1$. The SM strengths are multiplied by $1/10$. The total strengths denoted by the solid lines include both the $J = 1$ states with $K = 0$ and those with $K = \pm 1$, while the dotted and dashed lines show the $K = 0$ and $|K| = 1$ states, respectively.

cases, the μ dependence of the strength distribution is more substantial with increasing excess neutrons. In ^{90}Zr , the excitations are mainly built of the $2\hbar\omega_0$ excitation: $\mathcal{N} = 3 \rightarrow 5$ and $\mathcal{N} = 2 \rightarrow 4$. Among them, the $1f_{5/2} \rightarrow 1h_{11/2}$ excitation with $J = 3$ appears at low energy. In the $\mu = 0$ and -1 channels, the $0\hbar\omega_0$ excitation is also possible to occur: the particle-hole excitations from the $\nu 1g_{9/2}$ orbital within the $\mathcal{N} = 4$ shell. Furthermore, the $\nu 1g_{9/2} \rightarrow \pi 1g_{9/2}$ excitation participates in forming the low-lying states in the $\mu = -1$ channel. In ^{208}Pb , the $\pi 2d_{3/2} \rightarrow \nu 2g_{9/2}$ excitation with $J = 3$ and the $\pi 2d_{3/2} \rightarrow \nu 3d_{5/2}$ and $\pi 1h_{11/2} \rightarrow \nu 1j_{15/2}$ excitations generate the low energy states in the $\mu = +1$ channel. In the $\mu = 0$ and -1 channels, the $0\hbar\omega_0$ excitation is also available: the particle-hole excitations from the $\nu 1i_{13/2}$ orbital in the $\mathcal{N} = 6$ shell. Furthermore, the $\nu 1h_{11/2} \rightarrow \pi 1h_{11/2}$ excitation participates in forming the low-lying states in the $\mu = -1$ channel.

In these examples, one sees that the excitation energy of $J = 3$ is the lowest and $J = 1$ the highest. This is already seen in the unperturbed strength distributions and is consistent with the finding in the early study [6]. This is partly because the $J = 3$ states are constructed by the particle-hole excitation of the orbitals with $(\ell - 2)_{j_<}$ and $\ell_{j_>}$, whose unperturbed energy is lowered by the spin-orbit interaction. This explanation is similar to that quoted for the lowering of the $J = 2$ states of the spin dipole excitations [70].

2. Deformation effects

I am going to investigate the deformation effects. Figure 7 shows the GT and SM transition-strength distributions in

^{24}Mg and ^{28}Si . The total strengths denoted by the solid lines include the GT and SM transitions to both the $J = 1$ states with $K = 0$ and those with $K = \pm 1$, while the dotted and dashed lines depicting the $K = 0$ and $|K| = 1$ states, respectively. A large fraction of the SM strengths is found at low energy, where the GTR shows up. This characteristic feature is found in spherical nuclei as well [6,69]. As in the electric cases, the transition strength distributions in the three channels are similar to each other. Furthermore, the SM transition strengths in the $\mu = +1$ channel are enhanced because the Coulomb potential slightly expands the proton distribution, which leads to the asymmetry even in the $N = Z$ nuclei.

The strength distributions for $K = 0$ and $K = 1$ are different since the ground state is deformed. However, the K splitting does not show a “universal behavior” that the $K = 0$ states are shifted lower (higher) in energy in a prolate (oblate) deformed nucleus. This is because the GT operator does not change the spatial structure and the SM operator does not depend on the spatial direction. Furthermore, the ground state is time-even: $\langle \sigma_v \rangle = 0$. The K splitting occurring in the GT and SM excitations are due not to the collective deformation but to the underlying shell structure. In ^{24}Mg , the $K = 1$ states appear lower in energy than the $K = 0$ states, although the ground state is prolate deformed. The Fermi levels of neutrons and protons are both located in between the $[211]3/2$ and $[202]5/2$ orbitals. The $K = 1$ state is mainly generated by the $[211]3/2 \rightarrow [202]5/2$ and $[211]3/2 \rightarrow [211]1/2$ excitations, while the $K = 0$ state is constructed, e.g., by the $[220]1/2 \rightarrow [211]1/2$ excitation, both of which are far from the Fermi level. Thus, the $K = 1$ states appear lower in energy.

I then investigate the SQ excitations. Since the SQ operator involves the spherical harmonics $Y_{2\nu}(\hat{r})$, the K dependence can be attributed to nuclear deformation. However, the K quantum number is composed of the z component of angular momentum, reflecting the nuclear shape, and intrinsic spin; it is not apparent one should expect a direct correspondence between the K splitting and the nuclear deformation.

As discussed so far, the strength distributions in the $\mu = 0$ and ± 1 channels are similar to each other for the $N = Z$ light nuclei. Thus, I show in Fig. 8 the transition-strength distribution in the $\mu = +1$ channel only. One sees that the distributions for each K are different. The $K = 0$ ($K = 1$) strengths are enhanced in a prolate (oblate) deformed nucleus for $J = 1$. A universal feature of the K splitting can be seen for $J = 3$: the lower (higher)- K states appear lower in energy and possess enhanced strengths in a prolate (oblate) deformed nucleus. For $J = 2$, one sees that the $K = 2$ strengths appear in a relatively higher (lower) energy region in a prolate (oblate) deformed nucleus. However, it is not easy to distinguish the strength distributions of the other K for $J = 2$.

In the electric case, the K dependence of the transition strengths was evaluated qualitatively by looking at the NEWSR values using Eq. (11). The NEWSR values for the GT and SM excitations are the same as those assuming spherical symmetry (9): the spatial function $f(r)$ is constant for the GT operator, and that for the SM operator is r^2 , which is scalar. However, one needs to consider the K dependence for

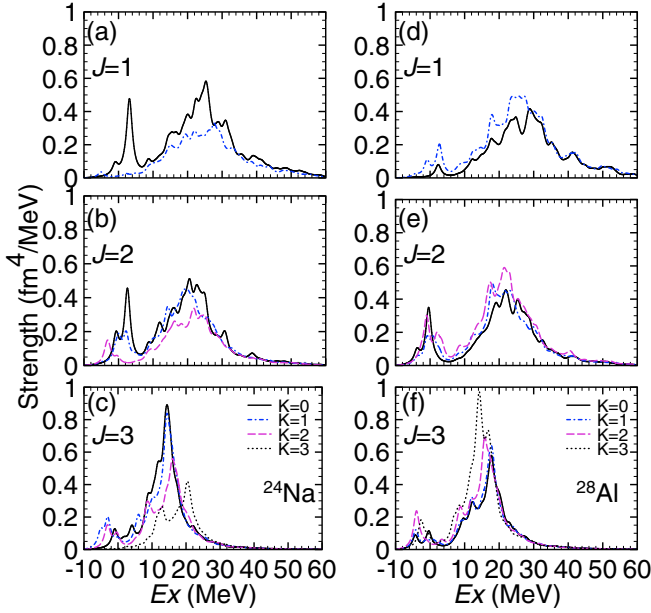


FIG. 8. As in Fig. 2 but for the spin-quadrupole (SQ) excitations in the $\mu = +1$ channel.

the SQ excitations. The NEWSR for the SQ excitations with (J, K) reads

$$m_{L=2(J,K)}^{-1} - m_{L=2(J,K)}^{+1} = \begin{cases} \frac{1}{8\pi} (N \langle 4z^4 + \rho^4 + 5\rho^2 z^2 \rangle_v - Z \langle \dots \rangle_\pi) & (1, 0), \\ \frac{1}{16\pi} (N \langle 2z^4 + 5\rho^4 + 7\rho^2 z^2 \rangle_v - Z \langle \dots \rangle_\pi) & (1, 1), \\ \frac{15}{8\pi} (N \langle \rho^2 z^2 \rangle_v - Z \langle \dots \rangle_\pi) & (2, 0), \\ \frac{5}{16\pi} (N \langle 2z^4 + \rho^4 - \rho^2 z^2 \rangle_v - Z \langle \dots \rangle_\pi) & (2, 1), \\ \frac{5}{16\pi} (N \langle \rho^4 + 2\rho^2 z^2 \rangle_v - Z \langle \dots \rangle_\pi) & (2, 2), \\ \frac{1}{16\pi} (N \langle 12z^4 + 3\rho^4 \rangle_v - Z \langle \dots \rangle_\pi) & (3, 0), \\ \frac{1}{32\pi} (N \langle 16z^4 + 5\rho^4 + 16\rho^2 z^2 \rangle_v - Z \langle \dots \rangle_\pi) & (3, 1), \\ \frac{5}{32\pi} (N \langle \rho^4 + 8\rho^2 z^2 \rangle_v - Z \langle \dots \rangle_\pi) & (3, 2), \\ \frac{15}{32\pi} (N \langle \rho^4 \rangle_v - Z \langle \dots \rangle_\pi) & (3, 3), \end{cases} \quad (13)$$

where $\langle \dots \rangle_\pi$ denotes the expectation value of the first term by replacing neutrons with protons. In deriving these sum rule values, I assume that J^π of the ground state of the mother nucleus is 0^+ ; the time-odd densities vanish in the ground state. For $J = 1$, the $K = 0$ ($K = 1$) strengths are characterized by a large $\langle z^4 \rangle$ ($\langle \rho^4 \rangle$) term. Since the prolate (oblate) deformation produces the large $\langle z^4 \rangle$ ($\langle \rho^4 \rangle$) value, the above finding can be reasonably understood. The “stretched” $J = 3$ excitation is relatively simple, particularly the $K = 0$ and $K = 3$ states. The prolate (oblate) deformation gives larger strengths in the

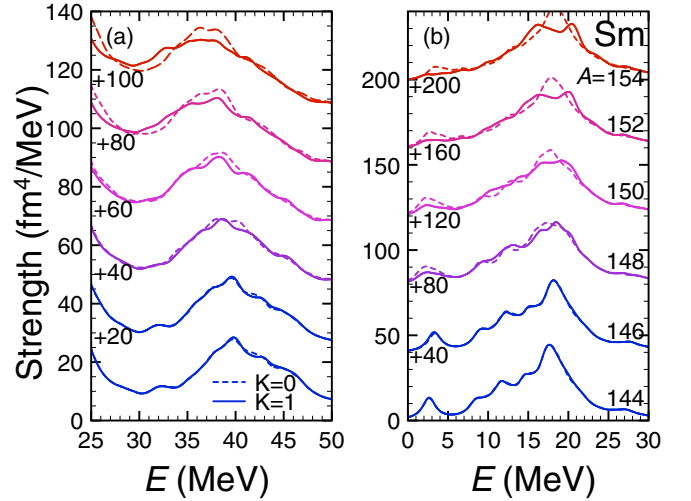


FIG. 9. As in Fig. 3 but for the spin-monopole (SM) excitations. The strengths for $K = 0$ and $K = 1$ are separately depicted by the dashed and solid lines, respectively.

$K = 0$ ($K = 3$) states. A similar feature has been found in the “stretched” $J = 2$ spin-dipole excitation in deformed nuclei though the K dependence is not clear for the $J = 0$ and $J = 1$ excitations [18].

According to the coupling between the monopole and the $K = 0$ component of the quadrupole excitations seen in the electric case, which is universal both in the IS and IV excitations, one is tempted to expect the spitting of the SM strengths to appear due to coupling to the $K = 0$ and $K = 1$ components of the SQ excitations in deformed nuclei. Figure 9 shows the SM transition strengths in the Sm isotopes with $A = 144$ – 154 . Here, the $K = 0$ and $K = 1$ strengths are displayed separately. It is hard to see the deformation effects in these distributions in either the $\mu = +1$ or $\mu = -1$ channels. One reason is that, for the electric quadrupole excitations, the $K = 0$ strengths are concentrated in a single peak; however, in the current case, the $K = 0$ and $K = 1$ strengths of the SQ excitations are widely spread out in 30–40 MeV depending on J . Another reason is that the SM strengths distribution is broadened irrespective of the nuclear shape, as shown in Fig. 10. The excitation energy of the SMR in the $\mu = +1$ channel is lower than that in the $\mu = -1$ channel from spherical to deformed nuclei, which follows the prediction made in Ref. [69] for spherical nuclei.

3. Dependence on the functional

The residual interaction in the spin-isospin channel plays a significant role in the IV spin excitations. To investigate the dependence of the IV magnetic GRs on the functional employed, I perform the calculation using the SkP functional [32], which has a property different from SkM*: the Landau parameter g'_0 of the SkM* and SkP functionals is 0.94 and 0.06, respectively [71].

Figure 10 shows the comparison of the calculated distributions of the SM excitation in $^{144,154}\text{Sm}$ obtained by using the SkM* and SkP functionals. In the $\mu = -1$ channel, the GT strength dominates over the SM strength at low energies

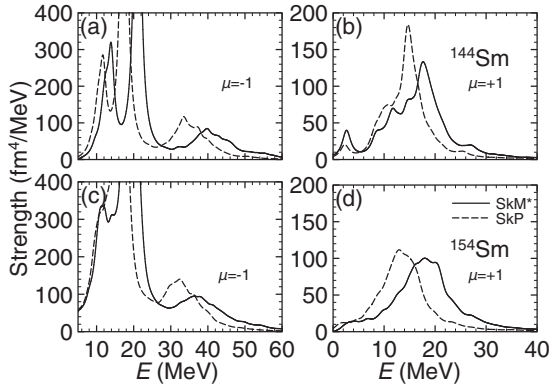


FIG. 10. Calculated distributions of the SM excitation in $^{144,154}\text{Sm}$ obtained using the SkM* and SkP functionals.

$E \lesssim 20$ MeV, and one finds the IVSMR around 30 and 40 MeV in the cases using the SkP and SkM* functionals, respectively. The excitation energy of the IVSMR in the $\mu = +1$ channel is calculated to be higher with the use of SkM* than SkP as in the $\mu = -1$ channel. The deformation makes the strength distribution smooth because the strength distributions for $K = 0$ and $K = 1$ are different; however, it does not produce the splitting.

Next, I discuss the functional dependence of the SQ excitation. Figure 11 shows the comparison of the calculated distributions of the SQ excitation in ^{144}Sm obtained by using the SkM* and SkP functionals. As observed above, the excitation energy of the $J = 3$ IVSQR is the lowest among $J = 1, 2,$ and 3 states. In all the cases, the excitation energy calculated by using SkM* is higher than that using SkP, whereas the calculated excitation energies of $J = 3$ states in the $\mu = +1$ channel are not very much different. I found that the RPA correlation is weak for the $J = 3$ SQ excitation in the $\mu = +1$ channel in ^{144}Sm ; the energy shift due to the residual interaction is small.

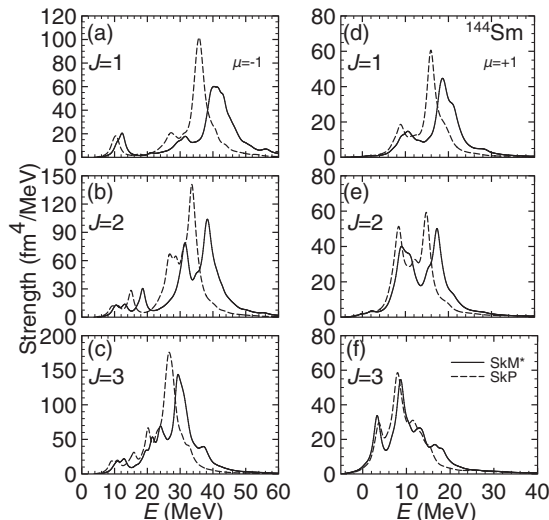


FIG. 11. As in Fig. 10 but for the SQ excitations in ^{144}Sm .

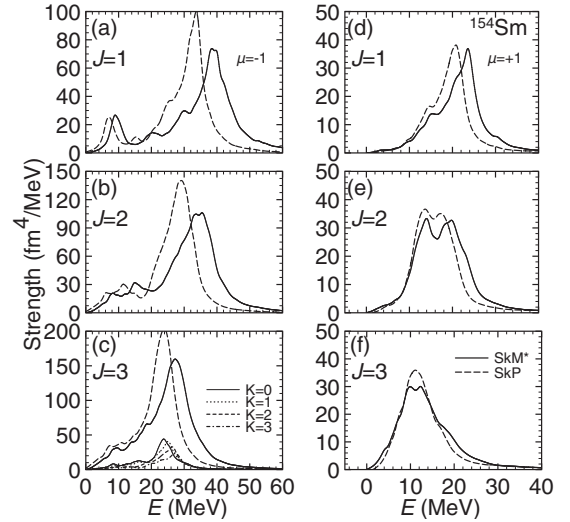


FIG. 12. As in Fig. 11 but for ^{154}Sm .

Finally, I investigate the functional dependence of the SQ excitations in deformed nuclei. As an example of the deformed nuclei, I show in Fig. 12 the comparison of the calculated distributions of the SQ excitation in ^{154}Sm obtained by using the SkM* and SkP functionals. The SkM* functional produces the IVSQR higher in energy than the SkP functional. Furthermore, as seen in the SM excitations in $^{144,154}\text{Sm}$, nuclear deformation makes the strength distribution smooth irrespective of the functional used. The $J = 3$ strengths for each K are displayed in Fig. 12(c) for SkP. One can see a universal behavior for the K splitting: the lower (higher) K states appear lower (higher) in energy and possess enhanced (reduced) strengths in a prolate deformed nucleus.

IV. SUMMARY

I have investigated the electric (non-spin-flip) and magnetic (spin-flip) IV monopole and quadrupole modes of excitation. To obtain the generic features of the IV excitations, the neutral ($\mu = 0$) and charge-exchange ($\mu = \pm 1$) channels have been considered simultaneously. Furthermore, I have explored open-shell nuclei to obtain unique features associated with nuclear deformation. To this end, I employed the nuclear energy-density functional (EDF) method: the Skyrme-Kohn-Sham-Bogoliubov and the quasiparticle random-phase approximation were used to describe the ground state and the transition to excited states.

A strong concentration of the monopole strengths in the energy region of the IAR has been found regardless of nuclear deformation. In addition, a resonance structure appears at high energy, which is generated mainly by particle-hole configurations with $2\hbar\omega_0$ excitation. The K splitting occurs in the electric quadrupole excitations due to deformation. The lower (higher) K states appear lower (higher) in energy in a prolate deformed nucleus, the opposite in an oblate deformed nucleus. Thus, the K splitting of the GQR is universal in the IS and IV excitations. Furthermore, the coupling to the

$K = 0$ component of the GQR brings about the splitting of the monopole strengths in all the channels of IV excitation.

Similarly to the electric excitations, I have found a strong concentration of the spin-monopole strengths in the energy region of the GTR regardless of nuclear deformation. The $J = 3$ states appear lowest in energy among the spin-quadrupole resonances. The K splitting occurs in the spin-monopole and spin-quadrupole excitations. However, the relation between the energy ordering depending on K and the deformation is not apparent: the K splitting in the spin-monopole excitation

is due to the change in the underlying shell structure similarly to the GTR, and that in the $J = 3$ spin-quadrupole resonance follows the universal trend.

ACKNOWLEDGMENTS

This work was supported by the JSPS KAKENHI (Grants No. JP19K03824 and No. JP19K03872). The numerical calculations were performed on Yukawa-21 at the Yukawa Institute for Theoretical Physics, Kyoto University.

-
- [1] M. Harakeh and A. Woude, *Giant Resonances: Fundamental High-frequency Modes of Nuclear Excitation*, Oxford Science Publications (Oxford University Press, Oxford, 2001).
- [2] B. L. Berman and S. C. Fultz, Measurements of the giant dipole resonance with monoenergetic photons, *Rev. Mod. Phys.* **47**, 713 (1975).
- [3] A. Bohr and B. Mottelson, *Nuclear Structure: Volume II, Nuclear Deformations* (Benjamin, Reading, MA, 1975).
- [4] N. Auerbach and A. Klein, A microscopic theory of giant electric isovector resonances, *Nucl. Phys. A* **395**, 77 (1983).
- [5] T. Izumoto, Giant spin-isospin vibrations and the continuum spectra from the (p,n) reaction at forward angles, *Nucl. Phys. A* **395**, 189 (1983).
- [6] N. Auerbach and A. Klein, Structure of isovector spin excitations in nuclei, *Phys. Rev. C* **30**, 1032 (1984).
- [7] F. Osterfeld, Nuclear spin and isospin excitations, *Rev. Mod. Phys.* **64**, 491 (1992).
- [8] H. Lenske, F. Cappuzzello, M. Cavallaro, and M. Colonna, Heavy ion charge exchange reactions as probes for nuclear β -decay, *Prog. Part. Nucl. Phys.* **109**, 103716 (2019).
- [9] S. S. Henshaw, M. W. Ahmed, G. Feldman, A. M. Nathan, and H. R. Weller, New Method for Precise Determination of the Isovector Giant Quadrupole Resonances in Nuclei, *Phys. Rev. Lett.* **107**, 222501 (2011).
- [10] X. Roca-Maza, M. Brenna, B. K. Agrawal, P. F. Bortignon, G. Colò, L.-G. Cao, N. Paar, and D. Vretenar, Giant quadrupole resonances in ^{208}Pb , the nuclear symmetry energy, and the neutron skin thickness, *Phys. Rev. C* **87**, 034301 (2013).
- [11] W. A. Sterrenburg, S. M. Austin, R. P. DeVito, and A. Galonsky, Q -Value Systematics for Isovector Giant Resonances Excited by (p, n) Reactions on Zr, Nb, Mo, Sn, and Pb Isotopes, *Phys. Rev. Lett.* **45**, 1839 (1980).
- [12] F. Krmpotić, K. Nakayama, and A. Galeão, Giant first-forbidden resonances, *Nucl. Phys. A* **399**, 478 (1983).
- [13] A. Krasznahorkay, N. Paar, D. Vretenar, and M. N. Harakeh, Neutron-skin thickness of ^{208}Pb from the energy of the anti-analogue giant dipole resonance, *Phys. Scr.* **T154**, 014018 (2013).
- [14] A. Krasznahorkay, N. Paar, D. Vretenar, and M. Harakeh, Anti-analog giant dipole resonances and the neutron skin of nuclei, *Phys. Lett. B* **720**, 428 (2013).
- [15] J. Yasuda, T. Wakasa, M. Okamoto, M. Dozono, K. Hatanaka, M. Ichimura, S. Kuroita, Y. Maeda, T. Noro, Y. Sakemi, M. Sasano, and K. Yako, Extraction of anti-analog giant dipole resonance and neutron skin thickness for ^{208}Pb , *Prog. Theor. Exp. Phys.* **2013**, 063D02 (2013).
- [16] L.-G. Cao, X. Roca-Maza, G. Colò, and H. Sagawa, Constraints on the neutron skin and symmetry energy from the anti-analog giant dipole resonance in ^{208}Pb , *Phys. Rev. C* **92**, 034308 (2015).
- [17] K. Yoshida, Charge-exchange dipole excitations in neutron-rich nuclei: $-1\hbar\omega_0$, anti-analog pygmy and anti-analog giant resonances, *Phys. Rev. C* **96**, 051302 (2017).
- [18] K. Yoshida, Charge-exchange dipole excitations in deformed nuclei, *Phys. Rev. C* **102**, 054336 (2020).
- [19] K. Yoshida, Pygmy dipole mode in deformed neutron-rich Mg isotopes close to the drip line, *Phys. Rev. C* **80**, 044324 (2009).
- [20] K. Yoshida, Roles of deformation and neutron excess on the giant monopole resonance in neutron-rich Zr isotopes, *Phys. Rev. C* **82**, 034324 (2010).
- [21] K. Yoshida and T. Nakatsukasa, Shape evolution of giant resonances in Nd and Sm isotopes, *Phys. Rev. C* **88**, 034309 (2013).
- [22] G. Scamps and D. Lacroix, Systematic study of isovector and isoscalar giant quadrupole resonances in normal and superfluid deformed nuclei, *Phys. Rev. C* **89**, 034314 (2014).
- [23] M. Kortelainen, N. Hinohara, and W. Nazarewicz, Multipole modes in deformed nuclei within the finite amplitude method, *Phys. Rev. C* **92**, 051302 (2015).
- [24] P. Vesely, J. Kvasil, V. O. Nesterenko, W. Kleinig, P. G. Reinhard, and V. Y. Ponomarev, Skyrme random-phase-approximation description of spin-flip $M1$ giant resonance, *Phys. Rev. C* **80**, 031302 (2009).
- [25] V. O. Nesterenko, P. I. Vishnevskiy, J. Kvasil, A. Repko, and W. Kleinig, Microscopic analysis of low-energy spin and orbital magnetic dipole excitations in deformed nuclei, *Phys. Rev. C* **103**, 064313 (2021).
- [26] U. Garg and G. Colò, The compression-mode giant resonances and nuclear incompressibility, *Prog. Part. Nucl. Phys.* **101**, 55 (2018).
- [27] M. Bender, P.-H. Heenen, and P.-G. Reinhard, Self-consistent mean-field models for nuclear structure, *Rev. Mod. Phys.* **75**, 121 (2003).
- [28] T. Nakatsukasa, K. Matsuyanagi, M. Matsuo, and K. Yabana, Time-dependent density-functional description of nuclear dynamics, *Rev. Mod. Phys.* **88**, 045004 (2016).
- [29] K. Yoshida and N. Van Giai, Deformed quasiparticle-random-phase approximation for neutron-rich nuclei using the Skyrme energy density functional, *Phys. Rev. C* **78**, 064316 (2008).
- [30] K. Yoshida, Spin-isospin response of deformed neutron-rich nuclei in a self-consistent Skyrme energy-density-functional approach, *Prog. Theor. Exp. Phys.* **2013**, 113D02 (2013).

- [31] K. Yoshida, Erratum: Spin–isospin response of deformed neutron-rich nuclei in a self-consistent Skyrme energy-density-functional approach, *Prog. Theor. Exp. Phys.* **2021**, 019201 (2021).
- [32] J. Dobaczewski, H. Flocard, and J. Treiner, Hartree-Fock-Bogolyubov description of nuclei near the neutron-drip line, *Nucl. Phys. A* **422**, 103 (1984).
- [33] H. Kasuya and K. Yoshida, Hartree–Fock–Bogoliubov theory for odd-mass nuclei with a time-odd constraint and application to deformed halo nuclei, *Prog. Theor. Exp. Phys.* **2021**, 013D01 (2021).
- [34] S. Ebata, T. Nakatsukasa, T. Inakura, K. Yoshida, Y. Hashimoto, and K. Yabana, Canonical-basis time-dependent Hartree-Fock-Bogoliubov theory and linear-response calculations, *Phys. Rev. C* **82**, 034306 (2010).
- [35] J. Bartel, P. Quentin, M. Brack, C. Guet, and H.-B. Håkansson, Towards a better parametrisation of Skyrme-like effective forces: A critical study of the SkM force, *Nucl. Phys. A* **386**, 79 (1982).
- [36] T. Peach, U. Garg, Y. K. Gupta, J. Hoffman, J. T. Matta, D. Patel, P. V. M. Rao, K. Yoshida, M. Itoh, M. Fujiwara, K. Hara, H. Hashimoto, K. Nakanishi, M. Yosoi, H. Sakaguchi, S. Terashima, S. Kishi, T. Murakami, M. Uchida, Y. Yasuda *et al.*, Effect of ground-state deformation on isoscalar giant resonances in ^{28}Si , *Phys. Rev. C* **93**, 064325 (2016).
- [37] M. Yamagami, Y. R. Shimizu, and T. Nakatsukasa, Optimal pair density functional for description of nuclei with large neutron excess, *Phys. Rev. C* **80**, 064301 (2009).
- [38] Y. Fujita, H. Fujita, T. Adachi, C. L. Bai, A. Algora, G. P. A. Berg, P. von Brentano, G. Colò, M. Csatlós, J. M. Deaven, E. Estevez-Aguado, C. Fransen, D. De Frenne, K. Fujita, E. Ganioglu, C. J. Guess, J. Gulyás, K. Hatanaka, K. Hirota, M. Honma *et al.*, Observation of Low- and High-Energy Gamow-Teller Phonon Excitations in Nuclei, *Phys. Rev. Lett.* **112**, 112502 (2014).
- [39] Y. Fujita, H. Fujita, T. Adachi, G. Susoy, A. Algora, C. L. Bai, G. Colò, M. Csatlós, J. M. Deaven, E. Estevez-Aguado, C. J. Guess, J. Gulyás, K. Hatanaka, K. Hirota, M. Honma, D. Ishikawa, A. Krasznahorkay, H. Matsubara, R. Meharchand, F. Molina *et al.*, High-resolution study of Gamow-Teller excitations in the $^{42}\text{Ca}(^3\text{He}, t)^{42}\text{Sc}$ reaction and the observation of a “low-energy super-Gamow-Teller state”, *Phys. Rev. C* **91**, 064316 (2015).
- [40] H. Fujita, Y. Fujita, Y. Utsuno, K. Yoshida, T. Adachi, A. Algora, M. Csatlós, J. M. Deaven, E. Estevez-Aguado, C. J. Guess, J. Gulyás, K. Hatanaka, K. Hirota, R. Hutton, D. Ishikawa, A. Krasznahorkay, H. Matsubara, F. Molina, H. Okamura, H. J. Ong *et al.*, Experimental study of Gamow-Teller transitions via the high-energy-resolution $^{18}\text{O}(^3\text{He}, t)^{18}\text{F}$ reaction: Identification of the low-energy “super”-Gamow-Teller state, *Phys. Rev. C* **100**, 034618 (2019).
- [41] K. Yoshida, Suddenly shortened half-lives beyond ^{78}Ni : $N = 50$ magic number and high-energy non-unique first-forbidden transitions, *Phys. Rev. C* **100**, 024316 (2019).
- [42] T. Nakatsukasa, P. Avogadro, S. Ebata, T. Inakura, and K. Yoshida, Self-consistent description of nuclear photoabsorption cross sections, *Acta Phys. Pol. B* **42**, 609 (2011).
- [43] K. Yoshida and T. Nakatsukasa, Dipole responses in Nd and Sm isotopes with shape transitions, *Phys. Rev. C* **83**, 021304 (2011).
- [44] K. Yoshida, N. Hinohara, and T. Nakatsukasa, Skyrme energy-density functional approach to collective dynamics, *J. Phys.: Conf. Ser.* **321**, 012017 (2011).
- [45] Y. Gupta, U. Garg, J. Matta, D. Patel, T. Peach, J. Hoffman, K. Yoshida, M. Itoh, M. Fujiwara, K. Hara, H. Hashimoto, K. Nakanishi, M. Yosoi, H. Sakaguchi, S. Terashima, S. Kishi, T. Murakami, M. Uchida, Y. Yasuda, H. Akimune *et al.*, Splitting of ISGMR strength in the light-mass nucleus ^{24}Mg due to ground-state deformation, *Phys. Lett. B* **748**, 343 (2015).
- [46] Y. Gupta, U. Garg, J. Matta, D. Patel, T. Peach, J. Hoffman, K. Yoshida, M. Itoh, M. Fujiwara, K. Hara, H. Hashimoto, K. Nakanishi, M. Yosoi, H. Sakaguchi, S. Terashima, S. Kishi, T. Murakami, M. Uchida, Y. Yasuda, H. Akimune *et al.*, Corrigendum to “Splitting of ISGMR strength in the light-mass nucleus ^{24}Mg due to ground-state deformation” [Phys. Lett. B 748 (2015) 343–346], *Phys. Lett. B* **751**, 597 (2015).
- [47] Y. K. Gupta, U. Garg, J. Hoffman, J. Matta, P. V. M. Rao, D. Patel, T. Peach, K. Yoshida, M. Itoh, M. Fujiwara, K. Hara, H. Hashimoto, K. Nakanishi, M. Yosoi, H. Sakaguchi, S. Terashima, S. Kishi, T. Murakami, M. Uchida, Y. Yasuda *et al.*, Deformation effects on isoscalar giant resonances in ^{24}Mg , *Phys. Rev. C* **93**, 044324 (2016).
- [48] K. Yoshida, Isovector spin susceptibility: Isotopic evolution of collectivity in spin response, *Phys. Rev. C* **104**, 014309 (2021).
- [49] K. Yoshida, Skyrme-QRPA calculations for low-lying excitation modes in deformed neutron-rich nuclei, *Eur. Phys. J. A* **42**, 583 (2009).
- [50] K. Yoshida and H. Watanabe, Enhanced collectivity of γ vibration in neutron-rich Dy isotopes with $N = 108$ – 110 , *Prog. Theor. Exp. Phys.* **2016**, 123D02 (2016).
- [51] H. Watanabe, G. Zhang, K. Yoshida, P. Walker, J. Liu, J. Wu, P. Regan, P.-A. Söderström, H. Kanaoka, Z. Korkulu, P. Lee, S. Nishimura, A. Yagi, D. Ahn, T. Alharbi, H. Baba, F. Browne, A. Bruce, R. Carroll, K. Chae *et al.*, Long-lived K isomer and enhanced γ vibration in the neutron-rich nucleus ^{172}Dy : Collectivity beyond double midshell, *Phys. Lett. B* **760**, 641 (2016).
- [52] G. Zhang, H. Watanabe, G. Dracoulis, F. Kondev, G. Lane, P. Regan, P.-A. Söderström, P. Walker, K. Yoshida, H. Kanaoka, Z. Korkulu, P. Lee, J. Liu, S. Nishimura, J. Wu, A. Yagi, D. Ahn, T. Alharbi, H. Baba, F. Browne *et al.*, Interplay of quasiparticle and vibrational excitations: First observation of isomeric states in ^{168}Dy and ^{169}Dy , *Phys. Lett. B* **799**, 135036 (2019).
- [53] K. Yoshida, Pairing and nonaxial-shape correlations in $N = 150$ isotones, *Phys. Rev. C* **104**, 024318 (2021).
- [54] E. Yüksel, N. Paar, G. Colò, E. Khan, and Y. F. Niu, Gamow-Teller excitations at finite temperature: Competition between pairing and temperature effects, *Phys. Rev. C* **101**, 044305 (2020).
- [55] W. Huang, M. Wang, F. Kondev, G. Audi, and S. Naimi, The AME 2020 atomic mass evaluation (I). Evaluation of input data, and adjustment procedures, *Chin. Phys. C* **45**, 030002 (2021).
- [56] M. Wang, W. Huang, F. Kondev, G. Audi, and S. Naimi, The AME 2020 atomic mass evaluation (II). Tables, graphs and references, *Chin. Phys. C* **45**, 030003 (2021).
- [57] G. Colò and N. Van Giai, Where is the non-spin-flip isovector monopole resonance in ^{208}Pb ?, *Phys. Rev. C* **53**, 2201 (1996).
- [58] A. Erell, J. Alster, J. Lichtenstadt, M. A. Moinester, J. D. Bowman, M. D. Cooper, F. Irom, H. S. Matis, E. Piaseczky, and

- U. Sennhauser, Measurements on isovector giant resonances in pion charge exchange, *Phys. Rev. C* **34**, 1822 (1986).
- [59] R. Pitthan, F. R. Buskirk, E. B. Dally, J. N. Dyer, and X. K. Maruyama, Electroexcitation of Giant Multipole Resonances in ^{197}Au and ^{208}Pb between 5 and 40 MeV Excitation Energy with 90-MeV Electrons, *Phys. Rev. Lett.* **33**, 849 (1974).
- [60] R. G. T. Zegers, A. M. van den Berg, S. Brandenburg, F. R. R. Fleuret, M. Fujiwara, J. Guillot, V. M. Hannen, M. N. Harakeh, H. Laurent, K. van der Schaaf, S. Y. van der Werf, A. Willis, and H. W. Wilschut, Search for Isovector Giant Monopole Resonances via the $\text{Pb}(^3\text{He}, tp)$ Reaction, *Phys. Rev. Lett.* **84**, 3779 (2000).
- [61] S. Nakayama, H. Akimune, Y. Arimoto, I. Daito, H. Fujimura, Y. Fujita, M. Fujiwara, K. Fushimi, H. Kohri, N. Koori, K. Takahisa, T. Takeuchi, A. Tamii, M. Tanaka, T. Yamagata, Y. Yamamoto, K. Yonehara, and H. Yoshida, Isovector Electric Monopole Resonance in ^{60}Ni , *Phys. Rev. Lett.* **83**, 690 (1999).
- [62] R. Leicht, M. Hammen, K. Schelhaas, and B. Ziegler, Absorption and scattering of photons by ^{208}Pb , *Nucl. Phys. A* **362**, 111 (1981).
- [63] K. Schelhaas, J. Henneberg, M. Sanzone-Arenhövel, N. Wieloch-Laufenberg, U. Zurmühl, B. Ziegler, M. Schumacher, and F. Wolf, Nuclear photon scattering by ^{208}Pb , *Nucl. Phys. A* **489**, 189 (1988).
- [64] D. S. Dale, R. M. Laszewski, and R. Alarcon, Isovector $E2$ Resonance in ^{208}Pb , *Phys. Rev. Lett.* **68**, 3507 (1992).
- [65] S. Fukuda and Y. Torizuka, Evidence for the giant monopole resonance in ^{90}Zr , *Phys. Lett. B* **62**, 146 (1976).
- [66] M. A. Godwin, E. Hayward, G. Feldman, L. H. Kramer, H. R. Weller, and W. R. Dodge, Isovector giant quadrupole resonance observed in $^{89}\text{Y}(\bar{p}, \gamma)^{90}\text{Zr}$, *Phys. Rev. C* **50**, 1528 (1994).
- [67] T. Ichihara, M. Ishihara, H. Ohnuma, T. Niizeki, Y. Satou, H. Okamura, S. Kubono, M. H. Tanaka, and Y. Fuchi, Isovector Quadrupole Resonance Observed in the $^{60}\text{Ni}(^{13}\text{C}, ^{13}\text{N})^{60}\text{Co}$ Reaction at $E/A = 100\text{MeV}$, *Phys. Rev. Lett.* **89**, 142501 (2002).
- [68] M. Scott, R. G. T. Zegers, R. Almus, S. M. Austin, D. Bazin, B. A. Brown, C. Campbell, A. Gade, M. Bowry, S. Galès, U. Garg, M. N. Harakeh, E. Kwan, C. Langer, C. Loelius, S. Lipschutz, E. Litvinova, E. Lunderberg, C. Morse, S. Noji *et al.*, Observation of the Isovector Giant Monopole Resonance via the $^{28}\text{Si}(^{10}\text{Be}, ^{10}\text{B}^*[1.74\text{ MeV}])$ Reaction at 100 AMeV, *Phys. Rev. Lett.* **118**, 172501 (2017).
- [69] I. Hamamoto and H. Sagawa, Charge-exchange spin monopole modes, *Phys. Rev. C* **62**, 024319 (2000).
- [70] G. Bertsch, D. Cha, and H. Toki, Systematics of the $\sigma\tau$ -strength in nuclei, *Phys. Rev. C* **24**, 533 (1981).
- [71] M. Bender, J. Dobaczewski, J. Engel, and W. Nazarewicz, Gamow-Teller strength and the spin-isospin coupling constants of the Skyrme energy functional, *Phys. Rev. C* **65**, 054322 (2002).